Transient Induced Voltages on Aboveground Pipelines Parallel to Overhead Transmission Lines

T. A. Papadopoulos, Z. G. Datsios, A. I. Chrysochos, A. G. Martins-Britto, G. K. Papagiannis

***Abstract*—Lightning strikes to conductors of overhead lines may cause high transient induced voltages at neighboring pipelines. Thus, the computation of these voltages is important for the safe and reliable pipeline operation. This work investigates the effects of line parameters and soil modelling on the transient voltages induced at an aboveground pipeline due to lightning strikes to a phase conductor of a nearby overhead transmission line. Three different earth formulations are evaluated: the Carson, Wise, and the method of moments with surface operator combined with the extended transmission line approaches. Computations are performed using both frequency- and time-domain models, as well as constant and frequency-dependent soil electrical properties. CIGRE lightning current waveforms are employed in simulations derived on the basis of the statistical distributions of their parameters for negative first return-strokes. Transient induced voltage waveforms differ among the evaluated lightning currents, with higher peak values for shorter and steeper current wavefronts. Conservative results are obtained for the constant soil properties and Carson's earth formulations, which neglect, respectively, the dispersion of soil electrical properties and displacement current.**

***Keywords*—Earth conduction effects, frequency-dependent soil models, overhead lines, pipelines, transients.**

I. Introduction

ROUTING pipelines and power lines in common right-of-ways results in electromagnetic interference (EMI) due to three mechanisms: (1) inductive or electromagnetic (EM), (2) capacitive or electrostatic, and (3) conductive coupling [1], [2]. Thus, voltages are transferred to pipelines which are the victim circuits, during steady-state conditions, power system faults, and transients, such as lightning strikes to the overhead lines (OHLs). Transferred voltages may pose a threat to people (danger of electric shock) and equipment (damages and aging) [1], [3]. Therefore, the assessment of voltages transferred to pipelines is important for safe and reliable operation, and has been a popular research subject during the last decades. However, most relevant studies deal with steady-state or fault conditions. A few papers investigate higher-frequency EMI between OHLs and pipelines [3], [4], [5].

High-frequency (HF) EMI, especially due to lightning strikes to OHLs, may cause significant induced voltages to aboveground pipelines [3]. For their computation, EM transient models are used employing per-unit-length self and mutual parameters between the line and the pipeline. These are affected significantly by the adopted earth formulation with several approaches proposed in literature, as summarized in [5]. These include the widely used Carson's approach [6], which is based on simplifying assumptions, and the more accurate earth approach proposed by Wise [7], [8]. Investigations on the transient performance of OHLs and gas-insulated buses have been performed using these approaches [9], [10]; however, the only study on the influence of earth conduction effects on HF EMI between OHLs and pipelines is [5], presenting results mostly on propagation characteristics and frequency-domain responses.

This work investigates the effects of line parameters and soil modelling on the transient voltages induced at an aboveground pipeline due to lightning strikes to a phase conductor of a nearby OHL. Three different earth formulations are assessed: the Carson [6], Wise [7], [8], and MoM-SO (method of moments with surface operator) [11], [12] combined with the extended transmission line [13] approach. Computations were performed using both frequency- and time-domain models. Constant and frequency-dependent (FD) soil models were evaluated. An accurate lightning first return-stroke current representation was considered. The stochastic nature of lightning is accounted for by investigating several lightning current waveforms derived according to the statistical distributions of their parameters.

II. Line parameters

The effects of the adopted approach for the calculation of the per-unit-length parameters of the configuration are evaluated on transient induced voltages affecting pipelines. The earth formulations considered are described in this section.

A. Wise/Carson integral form

According to the generalized earth formulation of Wise [7], [8] considering two conductors located above a homogeneous earth (see Fig. 1), the influence of earth conduction effects on the per-unit-length conductor parameters is described by the self and the mutual earth impedance, $Z'_{e_{ij}}$, and admittance, $Y'_{e_{ij}}$. The general form of these terms is [5], [7], [8]:

T. A. Papadopoulos is with the Power Systems Laboratory, Department of Electrical and Computer Engineering, Democritus University of Thrace, Xanthi 67100, Greece (e-mail of corresponding author: thpapad@ee.duth.gr).
Z. G. Datsios and G. K. Papagiannis are with the School of Electrical and Computer Engineering, Aristotle University of Thessaloniki, Thessaloniki 54124, Greece (e-mail: zdatsios@auth.gr, grigoris@eng.auth.gr).
Z. G. Datsios is also with the Department of Electrical and Computer Engineering, University of Western Macedonia, Kozani 50131, Greece.
A. I. Chrysochos is with Hellenic Cables, Maroussi 15125, Athens, Greece, (e-mail: achrysochos@hellenic-cables.com).
Amauri G. Martins-Britto is with LAPSE, Department of Electrical Engineering, University of Brasilia, Brasilia, Brazil, 70910-900 (e-mail: amaurigm@lapse.unb.br). .

Paper submitted to the International Conference on Power Systems Transients (IPST 2023) in Thessaloniki, Greece, June 12-15, 2023.

$$Z'_{e_{ij}} = \frac{j\omega\mu_0}{2\pi}\left(\ln\frac{D_{ij}}{d_{ij}} + \int_0^\infty F_e(\lambda)\cos\left(x_{ij}\lambda\right)d\lambda\right), \quad (1)$$

$$F_e(\lambda) = \frac{2\mu_g e^{-H_{ij}a_0}}{a_g\mu_0 + a_0\mu_g}, \quad (2)$$

$$Y'_{e_{ij}} = j\omega P_{e_{ij}}^{-1} = j\omega(P_{pg_{ij}} + P_{g_{ij}})^{-1}, \quad (3)$$

$$P_{e_{ij}} = \frac{1}{2\pi\varepsilon_0}\left(\ln\frac{D_{ij}}{d_{ij}} + \int_0^\infty Q_e\cos(x_{ij}\lambda)d\lambda\right), \quad (4)$$

$$Q_e = \frac{2\mu_g\gamma_0^2(\mu_0 a_0 + a_g\mu_g)e^{-H_{ij}a_0}}{(a_g\mu_0 + a_0\mu_g)\left(a_g\gamma_0^2\mu_g + a_0\gamma_g^2\mu_0\right)}, \quad (5)$$

where $D_{ij} = \sqrt{H_{ij}^2 + x_{ij}^2}$, $d_{ij} = \sqrt{(h_i - h_j)^2 + x_{ij}^2}$ and $H_{ij} = h_i + h_j$. The EM properties ε_0, μ_0, σ_0 are the permittivity, permeability and conductivity of air, respectively. The corresponding earth properties are $\varepsilon_g = \varepsilon_{rg}\varepsilon_0$, $\mu_g = \mu_{rg}\mu_0$ and σ_g; subscript r denotes relative quantities. The air and earth propagation constants are $\gamma_0 = jk_0 = j\omega\sqrt{\mu_0\varepsilon_0}$ and $\gamma_g = \sqrt{j\omega\mu_0\left(\sigma_g + j\omega\varepsilon_0\varepsilon_{rg}\right)}$. In (1)–(5), $a_0 = \lambda$ and $a_g = \sqrt{\lambda^2 + \gamma_g^2 + k_0^2}$.

From the generalized expressions of (1), (2), the well-known Carson's earth impedance formula can be derived by disregarding the displacement current in the air and the earth, referring to low-frequency (LF) applications (roughly up to some kHz). In this context, also the admittance earth conduction effects are neglected in (3) by disregarding the term described in (5). This earth approach is implemented in the routines of most EM transient software and is named hereafter as 'Carson's approach'.

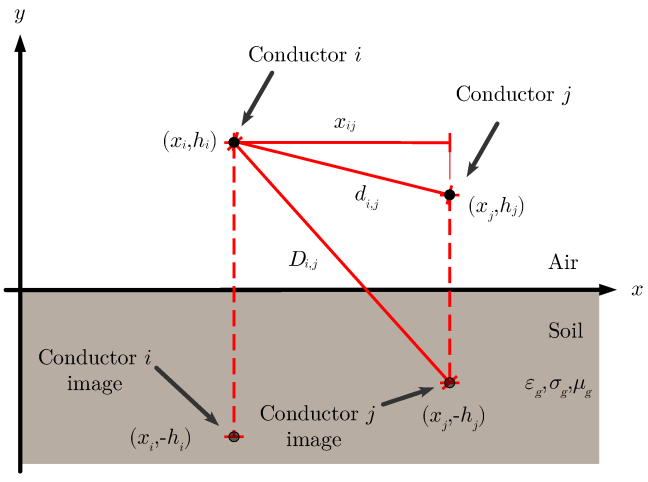

Fig. 1: Two conductors above imperfect homogeneous earth.

B. MoM-SO/ETL modelling

Alternative approaches to calculate the per-unit-length parameters of the configuration are by means of the finite element method (FEM), conductor partitioning, and MoM-SO [11]. MoM-SO is faster than FEM and conductor partitioning, as it does not require the meshing of the entire cross section of the system, but only at the conductors boundary [11]. In this method, conductors are represented through an equivalent current placed on their surface. By using a surface admittance operator and the Green's function of the surrounding medium, this representation allows for the computation of conductor impedance.

In [12], advances in the MoM-SO method regarding numerical instability for the case of OHLs were introduced. This implementation for the calculation of the internal and earth-return series impedances has been incorporated in the recent versions of the EMTP software [13], [14]. For the shunt admittance, a similar formulation to Wise's expressions has been used to take into account the influence of the imperfect earth [13]. This approach has been named as the 'extended transmission line' method (ETLM).

III. Simulation Models

The impact of the different formulations on the per-unit-length parameters is assessed in terms of transient induced voltages. For this purpose, state-of-the-art frequency- and time-domain transient simulation models are used.

A. Frequency-domain modelling

The frequency-domain transient model of [15] is employed, which is based on the generalized nodal methodology and the multi-conductor modal analysis [16]. The conventional algorithm of the numerical Laplace transform is used [17]. The model can be applied to all transmission line arrangements, since it properly incorporates the frequency dependence of the complex modal transformation matrix [18]. The major advantage of the model is the implementation of a high precision interpolation routine for the formulation of the nodal admittance matrix using a relatively small number of frequency data. This technique, combined with the utilization of a flexible sampling scheme, provides high accuracy in the simulation of any type of transients and great computational efficiency even in cases requiring high sampling rates.

B. Time-domain modelling

The time-domain modelling is based on the so-called universal line or wideband (WB) model [19], which is considered the most accurate for time-domain simulations of both OHLs and underground cables. The transmission line is characterized by the frequency-dependent propagation function and characteristic admittance. These matrices are fitted in phase-domain using the vector fitting algorithm in a state-space form [20] by encapsulating state-of-the-art techniques to generate a robust and accurate model [21]. The time delays of the propagation function are computed using Bode's formula [22] and optimized to minimize the fitting error using a search algorithm. Eventually, the time-domain

solution is performed in phase-domain using a delay-based circuit with Norton equivalents.

IV. Case Study

The system under study with main characteristics shown in Fig. 2 consists of a 150 kV, single-circuit, OHL in the close vicinity of a 10", carbon-steel, coated, aboveground pipeline.

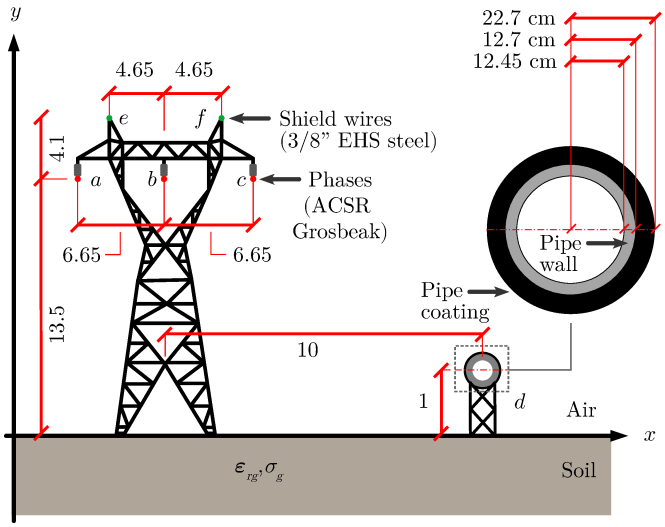

Fig. 2: Cross-section of the transmission line and the interfered pipeline. Dimensions in meters unless specified otherwise.

The OHL phase conductors (a, b, c) and shield wires (e, f) follow a parallel path with the pipeline (d) in the same right-of-way for 1000 m, defining the domain represented by the equivalent circuit of Fig. 3. Since the objective is to evaluate the responses in terms of propagation characteristics and transient induced voltages, all conductors are assumed to extend for several kilometers outside the parallel region without EMI exposures nor groundings (the effects of conductive couplings may be disregarded). Therefore, the OHL and the pipeline are nearly matched, by applying characteristic impedance terminations. In particular, the conductor terminations are represented with 574 Ω impedances for phases, 1354 Ω for shield wires and 306 Ω for the pipeline.

Three distinct soil models are analyzed in this paper: 1) constant properties (CP) model; 2) Longmire and Smith (LS) model; and 3) CIGRE WG C4.33 model. In the CP model, the soil is described by its frequency-invariant base properties, namely, LF conductivity $\sigma_{g,LF} = 0.01$ or 0.001 S/m and $\varepsilon_{rg} = 15$ or $\varepsilon_{rg} = 5$, respectively.

The LS is a FD soil model based on laboratory measurements within 100 Hz – 200 MHz, with earth permittivity ε_{rg} and conductivity σ_g (S/m) determined as [23]:

$$\varepsilon_{rg}(f) = \varepsilon_{rg,\infty} + \sum_{n=1}^{13} \frac{a_n}{1 + (f/f_n)^2}, \tag{6}$$

$$\sigma_g(f) = \sigma_{g,DC} + 2\pi f \varepsilon_0 \sum_{n=1}^{13} \frac{a_n f/f_n}{1 + (f/f_n)^2}, \tag{7}$$

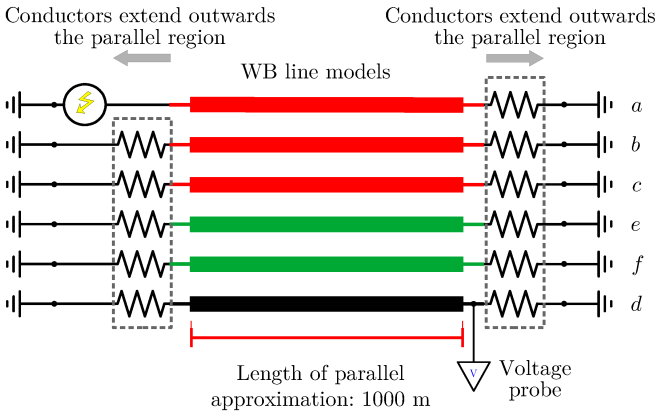

Fig. 3: Equivalent circuit representation of the parallel section under study.

in which f (Hz) is the frequency, $\varepsilon_{rg,\infty}$ is the HF relative permittivity of soil (equal to 5), a_n (p.u.) are empirical coefficients given in Table I of [23], and f_n (Hz) are scaling coefficients calculated as a function of the DC soil conductivity, $\sigma_{g,DC}$ (S/m):

$$f_n = 10^{n-1}(125\sigma_{g,DC})^{0.8312}. \tag{8}$$

In the CIGRE model, derived on the basis of field measurements and valid for the frequency spectrum of 100 Hz – 4 MHz, the corresponding ε_{rg} and σ_g equations are [24]:

$$\varepsilon_{rg}(f) = 12 + 9.5 \cdot 10^4 \sigma_{g,LF}^{0.27} f^{-0.46}, \tag{9}$$

$$\sigma_g(f) = \sigma_{g,LF} + 4.7 \cdot 10^{-6} \sigma_{g,LF}^{0.27} f^{0.54}, \tag{10}$$

in which $\sigma_{g,LF}$ (S/m) is the soil conductivity at 100 Hz.

Fig. 4 shows the variation of the electrical properties of soil with frequency as predicted by the LS (6) - (8) and CIGRE (9), (10) models. The cases considered in this study are depicted: $\sigma_{g,LF} = 0.01$ S/m and 0.001 S/m. Both soil models yield an increasing σ_g with increasing frequency; the opposite is true for the relative permittivity ϵ_{rg}, which decreases rapidly. It is evident that the CIGRE soil model yields a more marked increase of conductivity with frequency, even though the soil for the LS model is more conductive for $\sigma_{g,LF} = 0.01$ S/m. In addition, a less pronounced decrease of ϵ_{rg} for the CIGRE model can be observed.

First, the propagation characteristics, namely, the attenuation constants and phase velocities are investigated for $\sigma_{g,LF} = 0.001$ S/m, in order to establish an understanding of the system behavior. The Levenberg–Marquardt algorithm coupled with an eigenvector correlation technique was used to prevent switchovers in the frequency-domain [18]. The phase conductors, pipeline and shield wires listed from a to f in Fig. 3 have been mapped to six decoupled propagation modes, numbered from #1 to #6, with the characteristics described in Fig. 5, assuming CP soil and Wise's model [7], [8].

The figure indicates the presence of four aerial modes associated with the shield wires (#1 and #2) and the phase

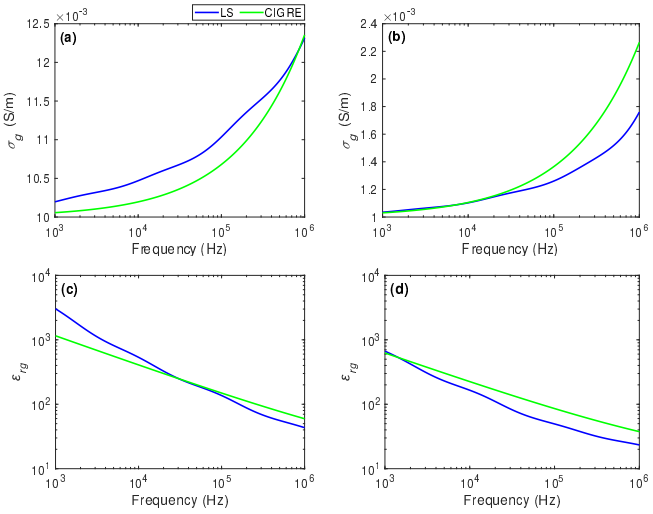

Fig. 4: Frequency spectra of the electrical properties of soil predicted using the LS and CIGRE soil models. (a), (b) Conductivity, σ_g , for $\sigma_{g,LF} = 0.01$ S/m and 0.001 S/m, respectively, and (c), (d) the corresponding variation of the relative permittivity ε_{rg}.

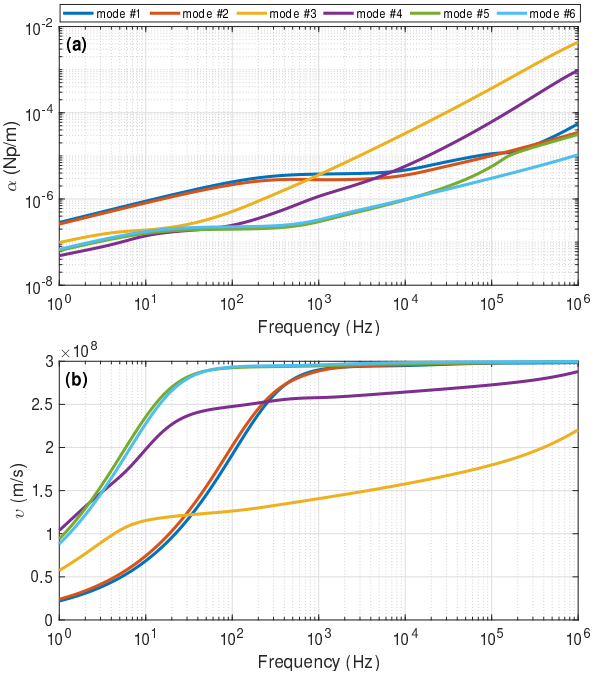

Fig. 5: Modal (a) attenuation constant and (b) velocity using Wise's formula and CP soil model, $\sigma_{g,LF} = 0.001$ S/m [5].

conductors (#5 and #6). These modes show similar pair-wise trends, but the shield wire modes attenuate more steeply and propagate slower than the corresponding phase counterparts. Mode #3 corresponds to the pure ground mode along a lossy medium, as the high attenuation and lowest phase velocities suggest. Finally, mode #4 is associated to the metallic pipeline, which is characterized by high attenuation due to the effect of the ground return impedance, and high propagation velocity, since conduction also involves the pipeline itself.

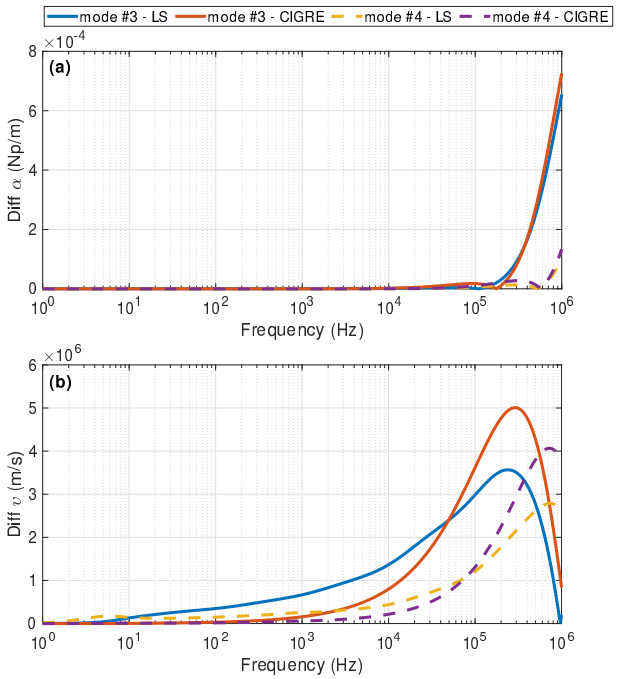

Fig. 6: Differences in the modal (a) attenuation constant and (b) velocity for the pure ground (mode #3, solid lines) and the pipeline (mode #4, dashed lines) for the FD soil models compared with the CP soil model, with $\sigma_{g,LF} = 0.001$ S/m.

From the very definition of modal decomposition [18], it follows that the existence of a pipeline mode will result in induced voltages along the pipeline due to EM and electrostatic coupling mechanisms, in the event of a phase energization. Even though this is well-established knowledge in the specialized EMI literature [1], inspection of the curves for mode #4 in Fig. 5 indicates that, as far as transient phenomena are concerned, pipeline voltages should respond differently to distinct harmonic components, especially in the HF spectrum. This effect becomes more pronounced when the soil properties FD nature is considered as shown in Fig. 6; where the absolute deviation of mode #3 and #4 propagation characteristics for the LS and the CIGRE FD soil models is presented with respect to those of the CP model.

V. Transient Results

To offer a practical perspective about the effects of line parameters and soil modelling on pipeline induced voltages, a lightning impact study is carried out with time-domain simulations. An accurate lightning return-stroke current representation is considered accounting for its actual stochastic nature. The effects of the earth formulation, line modelling and soil model are analyzed.

A. Lightning current waveforms

As shown in Fig. 3, lightning strikes to the outer phase conductor (shielding failure) of the 150 kV OHL of Fig. 2 were considered in transient simulations. The lightning current waveform introduced by CIGRE WG 33.01 [25] was adopted. Its front is upwardly concave, as in directly recorded

lightning return-stroke currents. In detail, two expressions are employed for lightning current generation, one up to the point of maximum steepness at the front (90% of the peak current), and a double-exponential expression from this point up to the peak, as well as for the wavetail. The disadvantage of this approach is the discontinuous current derivative at the transition point between expressions; the latter may affect results in specific cases, e.g., induced effects.

Using the methodology of [26] for the electrogeometric lightning attachment model of IEEE Std 1243 [27], a maximum shielding failure current, I_{MSF}, of 5.8 kA was calculated for the outer phase conductors of the 150 kV line. I_{MSF} calculations were performed at average conductor height. It is noted that I_{MSF} is the highest lightning peak current associated with first return-strokes that could terminate to the phase conductor of a shielded OHL. A lightning current of 5 kA ($< I_{MSF}$) was selected to be employed in simulations to result in withstand of the insulation of the 150 kV line. The critical lightning current causing shielding failure flashover was found equal to 5.2 kA through ATP-EMTP simulations using the modelling technique of [28]. It is important that lightning return-stroke current injected to a phase conductor is divided evenly in the two directions of the OHL. Hence, 2.5 kA were considered flowing in each direction of the outer phase conductor in this work. This value corresponds to an infinite lightning channel equivalent impedance (ideal lightning current source), adopted here to facilitate investigations. This is appropriate for lightning strikes with relatively low peak current, as lightning channel impedance is generally considered to increase with decreasing lightning current taking values higher than 1 kΩ for currents < 20 kA [29].

Five first return-stroke current waveforms of negative downward lightning flashes were investigated in this work with parameters listed in Table I. These were derived by considering the log-normal approximations of their statistical distributions [25], [30]. The first waveform (called "Median") corresponds to the median values of the front time (t_{d30}), maximum steepness (S_m), and time to half value (t_h). For the remaining four waveforms, one parameter, t_{d30} or S_m, was changed at a time taking a value exceeded by 5% or 95% of cases (Table I). t_h was kept constant for all investigated waveforms as it is expected to have a smaller influence on simulation results. The statistical distributions of [25] for the front time and maximum steepness are conditional for a given lightning peak current; the values of t_{d30} and S_m of Table I refer to 5 kA and were calculated as in [30]. Finally, a 2.5 kA, 1.2/50 μs waveform was employed in simulations for comparison purposes, as such standard lightning impulse (LI) waveforms are commonly used in relevant studies.

Waveforms are shown in Fig. 7 to facilitate comparisons. There is a significant influence of the statistical variation of the front time on the lightning current (F95, Median, and F5 waveforms of Fig. 7), also affecting its frequency content. On the other hand, the effect of the maximum steepness is relatively small (S95, Median, and S5 waveforms of Fig. 7). Also, the front of the LI waveform is different in shape exhibiting the shortest time to peak value.

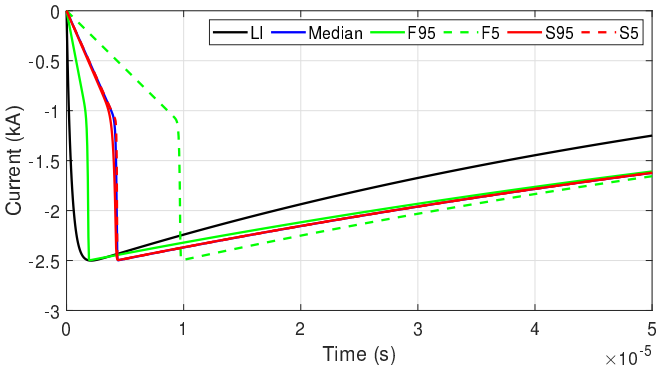

Fig. 7: Examined lightning return-stroke current waveforms.

TABLE I: Examined lightning current waveforms

Waveform	Description	t_{d30} (μs)	S_m (kA/μs)	t_h (μs)
Median	Median values for all parameters	2.40	15.80	77.5
F95	t_{d30} exceeded by 95% of cases	1.06	15.80	
F5	t_{d30} exceeded by 5% of cases	5.40		
S95	S_m exceeded by 95% of cases	2.40	6.35	
S5	S_m exceeded by 5% of cases		39.31	
LI	1.2/50 μs double-exponential waveform		–	

Median, F95, F5, S95, and S5: CIGRE [25] waveforms; parameters definitions and statistical distributions according to [25]; t_{d30}: front time, S_m: maximum steepness, and t_h: time to half value.

B. Impact of earth formulation

To assess the impact of the different earth formulations on HF EMI phenomena, pipeline transient voltages at the receiving end are given in Fig. 8 for $\sigma_{g,LF} = 0.001$ S/m, with comparisons of Carson, Wise and MoM-SO/ETLM approaches. The transient responses are calculated by using the frequency-domain (Laplace) simulation model. Results show that Carson's model yields increased (more conservative) results at the dominant peak value, whereas Wise's and MoM-SO/ETLM curves practically overlap along the entire transient duration. The difference between Carson's and Wise, MoM-SO/ETLM results are explained by the fact that Carson's earth model entirely neglects earth displacement current, which plays an important role in the pipeline mode attenuation, especially within the upper frequency spectrum [5]. On the other hand, Wise and MoM-SO/ETLM properly handle the earth permittivity in the calculation of the line and the pipeline parameters, thus providing a more realistic approach.

From Fig. 8 it can also be seen that the peak value of the transient voltage at the receiving end of the pipeline increases for shorter and steeper lightning current wavefronts. The highest voltage value was obtained for the LI waveform (shortest front) and the lowest for the F5 waveform (longest front), in line with Fig. 7. In addition, the computed voltage peak values for the Median, S95, and S5 waveforms are almost equal, as differences among these lightning currents are insignificant (Fig. 7); nevertheless, differences in the transient

voltage shape can be observed. However, it should be noted that the statistical distribution of the maximum steepness is conditional for a given lightning peak current and, hence, maximum steepness effects may be enhanced for higher lightning currents. In addition, it is important that the above also hold for the results of sections V-C and V-D.

It is noteworthy that for the CIGRE waveforms a "spike" may be obtained on the front of the transient voltages of Fig. 8 at the point right after the initial slower voltage increase and before the voltage steepness becomes higher. This is attributed to the transition between the two expressions used to describe the lightning current according to CIGRE [25].

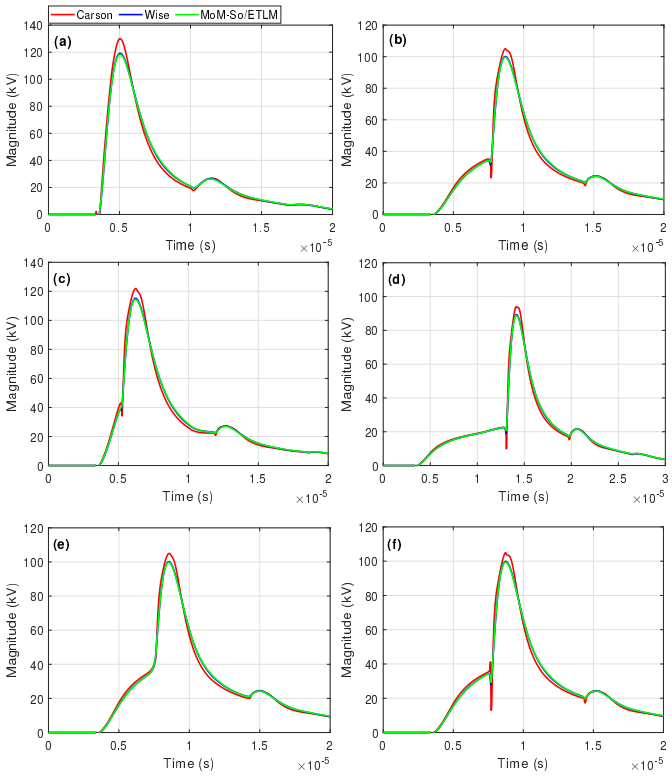

Fig. 8: Effect of earth formulation on the induced voltage at the pipeline receiving end, $\sigma_{g,LF} = 0.001$ S/m. Waveform: (a) LI, (b) Median, (c) F95, (d) F5, (e) S95, (f) S5.

C. Impact of simulation model

The transient voltages at the receiving end of the pipeline are compared in Fig. 9 using both frequency- (Laplace) and time-domain (WB) models for all lightning current waveforms of Table I. Results are calculated for $\sigma_{g,LF} = 0.001$ S/m and the per-unit-length parameters are based on Wise's earth approach considering the CP soil model. It is evident that the transient overvoltages of all cases are in excellent agreement between the two simulation models, as the normalized root-mean-square deviation ranges from 0.086% to 0.1205%, validating their use in the calculation of transient phenomena.

D. Effect of soil modelling

In Figs. 10 and 11, the transient voltages at the receiving end of the pipeline are summarized for all lightning

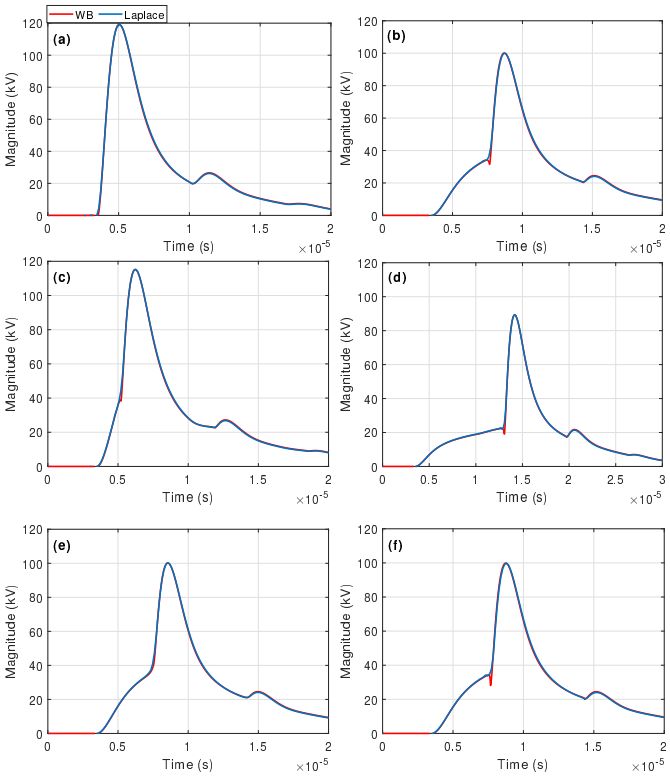

Fig. 9: Effect of simulation model on the induced voltage at the pipeline receiving end, $\sigma_{g,LF} = 0.001$ S/m. Waveform: (a) LI, (b) Median, (c) F95, (d) F5, (e) S95, (f) S5.

current waveforms, assuming $\sigma_{g,LF} = 0.01$ S/m and $\sigma_{g,LF} = 0.001$ S/m, respectively. The earth parameters of the OHL/pipeline configuration are calculated by Wise's earth approach considering the CP and the two FD soil models described in Section IV; the frequency-domain (Laplace) simulation model has been used. The absolute deviations between the FD soil models and the CP model are summarized for all above cases in Fig. 12.

In Fig. 12 the differences in the voltage waveforms of Figs. 10 and 11 are apparent at the first induced voltage peak, with the CP soil model yielding higher peak values (conservative results). Noticeable deviations of the FD soil model peak voltage values from those of the CP model are mostly observed for the poorly conductive soil (Fig. 11), due to the increasing effect of the soil resistivity dispersion and displacement current [5], [31]. These deviations become more pronounced for the lightning current waveforms with shorter and steeper fronts (higher frequency content) in agreement with the results on the propagation characteristics presented in [5]. In fact, the largest and smallest differences between CP and FD soil model results are observed respectively for the LI and F5 waveform (Fig. 7).

From Figs. 10, 11 and 12, it is evident that the results of the LS and the CIGRE FD soil models are similar for both soil cases and all examined lightning waveforms. Small and insignificant differences are observed, even though these soil models yield different frequency spectra of soil electrical properties as seen in Fig. 4.

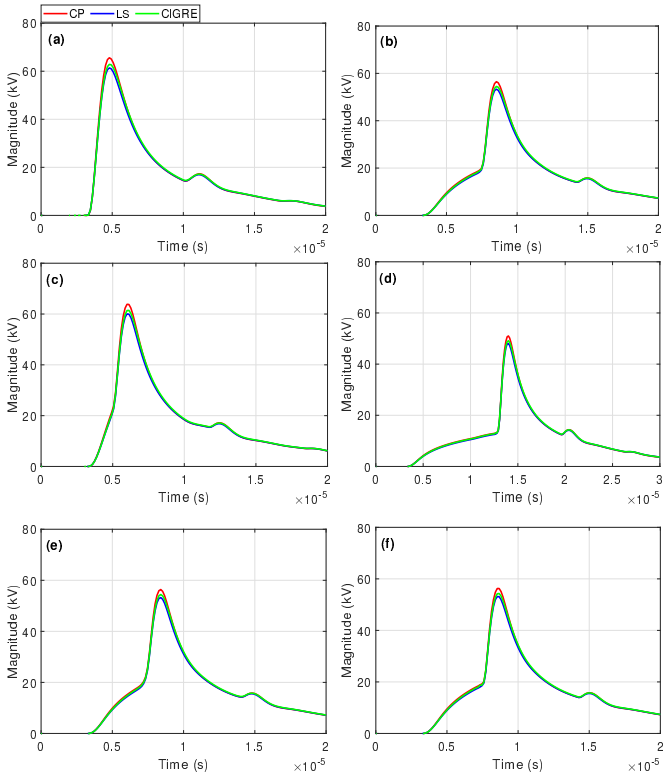

Fig. 10: Effect of soil modelling on the transient induced voltage at the pipeline receiving end, $\sigma_{g,LF} = 0.01$ S/m. Waveform: (a) LI, (b) Median, (c) F95, (d) F5, (e) S95, (f) S5.

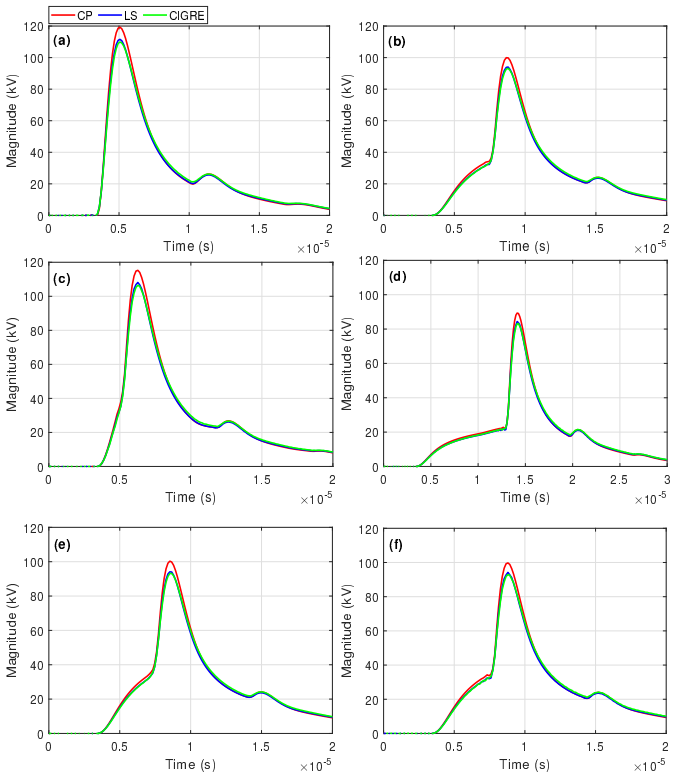

Fig. 11: Effect of soil modelling on the transient induced voltage at the pipeline receiving end, $\sigma_{g,LF} = 0.001$ S/m. Waveform: (a) LI, (b) Median, (c) F95, (d) F5, (e) S95, (f) S5.

VI. Conclusions

The effects of line parameters and soil modelling on the transient voltages induced on an aboveground pipeline due to lightning strikes at a phase conductor of a nearby overhead transmission line have been investigated. The earth formulations of Carson, Wise, and MoM-SO/ETLM have been evaluated. Computations were performed using both frequency- and time-domain models and by adopting constant and frequency-dependent (FD) soil electrical properties, considering two widely used FD soil models proposed by Longmire and Smith and CIGRE WG C4.33. An accurate lightning first return-stroke current representation, as proposed by CIGRE WG 33.01, is employed in simulations. The stochastic nature of lightning is accounted for by investigating several lightning current waveforms derived on the basis of the statistical distributions of their parameters.

Carson's earth formulation yields conservative (higher) transient induced voltage peak values, as it disregards the displacement current. An excellent agreement was found between the induced voltage waveforms obtained for Wise and MoM-SO/ETLM approaches, which practically overlap along the entire transient duration. These approaches, taking into account conduction effects on series impedances and shunt admittances, are considered as more realistic. Regarding the simulation models employed in transient induced voltage computations, the same results were obtained using the Laplace and the wideband models. This validates their use in the electromagnetic transient simulations.

Higher peak values of transient induced voltages were observed for soil models with constant electrical properties when compared with the results of FD soil models. Deviations become more pronounced for poorly conductive soils due to the increasing effect of the soil resistivity dispersion and displacement current. The differences between the induced voltage waveforms computed for the two FD soil models are small and insignificant, despite the deviations in the frequency spectra of soil electrical properties predicted by these models.

The transient induced voltages affecting the pipeline exhibit higher peak values for shorter and steeper lightning current wavefronts (higher frequency content). The highest peak voltages were found for the LI 1.2/50 μs double-exponential waveform, as its time to peak is much shorter than that of the realistic lightning first return-stroke current waveforms. When evaluating the statistical variation of the lightning current waveform parameters, it can be concluded that the front time affects considerably the induced voltage waveforms, whereas the effect of the maximum steepness is insignificant. The latter, however, may be enhanced for higher lightning currents.

References

[1] "CIGRE WG 36.02. guide concerning influence of high voltage AC power systems on metallic pipelines," *CIGRE TB 95*, pp. 1–44, 1995.

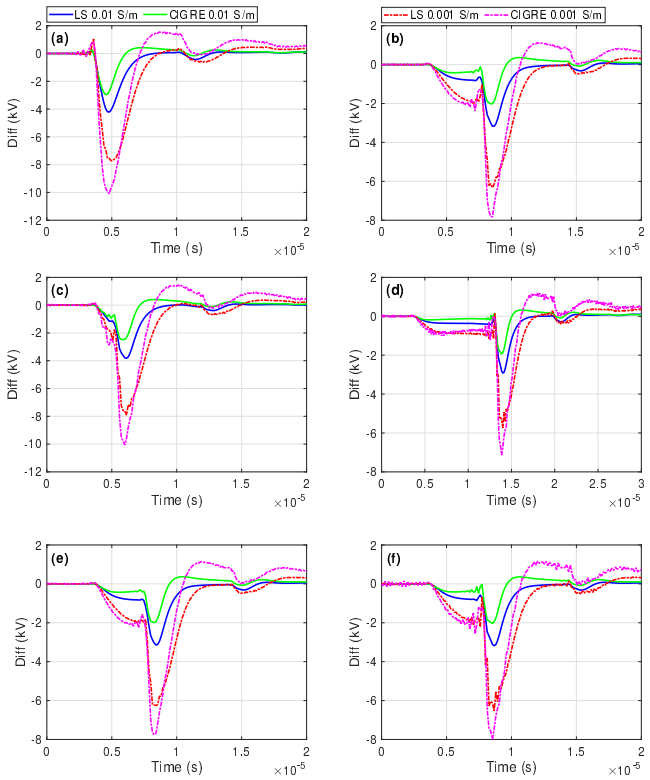

Fig. 12: Differences of the LS and CIGRE soil models with respect to CP model on the pipeline induced voltages, for $\sigma_{g,LF} = 0.01$ S/m and $\sigma_{g,LF} = 0.001$ S/m. Waveform: (a) LI, (b) Median, (c) F95, (d) F5, (e) S95, (f) S5.

[2] F. P. Dawalibi and R. D. Southey, "Analysis of electrical interference from power lines to gas pipelines. Part I: Computation methods," *IEEE Trans. Power Del.*, vol. 4, no. 3, pp. 1840–1846, 1989.

[3] K. Kopsidas and I. Cotton, "Induced voltages on long aerial and buried pipelines due to transmission line transients," *IEEE Trans. Power Del.*, vol. 23, no. 3, pp. 1535–1543, 2008.

[4] A. G. Martins-Britto, C. M. Moraes, and F. V. Lopes, "Transient electromagnetic interferences between a power line and a pipeline due to a lightning discharge: An EMTP-based approach," *Electr. Power Syst. Res.*, vol. 197, p. 107321, 2021.

[5] A. G. Martins-Britto, T. A. Papadopoulos, Z. G. Datsios, A. I. Chrysochos, and G. K. Papagiannis, "Influence of lossy ground on high-frequency induced voltages on aboveground pipelines by nearby overhead transmission lines," *IEEE Trans. Electromagn. Compat.*, vol. 64, no. 6, pp. 2273–2282, 2022.

[6] J. Carson, "Wave propagation in overhead wires with ground return," *Bell Syst. Tech. J.*, pp. 539–554, 1926.

[7] W. H. Wise, "Propagation of high-frequency currents in ground return circuits," *Proc. Inst. Radio Eng.*, vol. 22, no. 4, pp. 522–527, 1934.

[8] ——, "Potential coefficients for ground return circuits," *Bell Syst. Tech. J.*, vol. 27, no. 2, pp. 365–371, 1948.

[9] T. A. Papadopoulos, G. K. Papagiannis, and D. P. Labridis, "A generalized model for the calculation of the impedances and admittances of overhead power lines above stratified earth," *Electr. Power Syst. Res.*, vol. 80, pp. 1160–1170, 2010.

[10] H. M. J. De Silva, Z. Liu, D. Muthumuni, and A. Ametani, "EMT simulation of very-fast transients in gas-insulated substations using modified Carson's formula," *IEEE Trans. Electromagn. Compat.*, vol. 63, no. 4, pp. 1258–1265, 2021.

[11] U. R. Patel and P. Triverio, "MoM-SO: A complete method for computing the impedance of cable systems including skin, proximity, and ground return effects," *IEEE Trans. Power Del.*, vol. 30, no. 5, pp. 2110–2118, 2015.

[12] H. Xue, A. Ametani, J. Mahseredjian, and I. Kocar, "Computation of overhead line/underground cable parameters with improved MoM-SO method," in *2018 Power Systems Computation Conference (PSCC)*, 2018, pp. 1–7.

[13] H. Xue, A. Ametani, J. Mahseredjian, and I. Kocar, "Generalized formulation of earth-return impedance/admittance and surge analysis on underground cables," *IEEE Transactions on Power Delivery*, vol. 33, no. 6, pp. 2654–2663, 2018.

[14] "EMTP-RV Simulation Software," vol. http://www.emtp.com, accessed 15 October 2022.

[15] A. I. Chrysochos, T. A. Papadopoulos, and G. K. Papagiannis, "Enhancing the frequency-domain calculation of transients in multiconductor power transmission lines," *Electr. Power Syst. Res.*, vol. 122, pp. 56–64, 2015.

[16] L. M. Wedepohl, "Application of matrix methods to the solution of travelling-wave phenomena in polyphase systems," *Proc. Inst. Elect. Eng.*, vol. 110, no. 12, pp. 2200–2212, 1963.

[17] P. Moreno and A. Ramirez, "Implementation of the numerical Laplace transform: A review," *IEEE Trans. Power Del.*, vol. 23, no. 4, pp. 2599–2609, 2008.

[18] A. I. Chrysochos, T. A. Papadopoulos, and G. K. Papagiannis, "Robust calculation of frequency-dependent transmission-line transformation matrices using the Levenberg-Marquardt method," *IEEE Trans. Power Del.*, vol. 29, no. 4, pp. 1621–1629, 2014.

[19] A. Morched, B. Gustavsen, and M. Tartibi, "A universal model for accurate calculation of electromagnetic transients on overhead lines and underground cables," *IEEE Trans. Power Del.*, vol. 14, no. 3, pp. 1032–1038, 1999.

[20] B. Gustavsen and A. Semlyen, "Rational approximation of frequency domain responses by vector fitting," *IEEE Trans. Power Del.*, vol. 14, no. 3, pp. 1052–1061, 1999.

[21] I. Kocar, J. Mahseredjian, and G. Olivier, "Weighting method for transient analysis of underground cables," *IEEE Trans. Power Del.*, vol. 23, no. 3, pp. 1629–1635, 2008.

[22] I. Kocar and J. Mahseredjian, "New procedure for computation of time delays in propagation function fitting for transient modeling of cables," *IEEE Trans. Power Del.*, vol. 31, no. 2, pp. 613–621, 2016.

[23] C. Longmire and K. Smith, "A universal impedance for soils," *DNA 3788T, Mission Research Corp., Santa Barbara, CA*, 1975.

[24] "CIGRE WG C4.33. Impact of soil-parameter frequency dependence on the response of grounding electrodes and on the lightning performance of electrical systems," *CIGRE TB 781*, 2019.

[25] "CIGRE WG 33.01. Guide to procedures for estimating the lightning performance of transmission lines," *CIGRE TB 63*, 1991.

[26] P. N. Mikropoulos and T. E. Tsovilis, "Lightning attachment models and maximum shielding failure current of overhead transmission lines: Implications in insulation coordination of substations," *IET Gener. Transm. Distrib.*, vol. 4, no. 12, pp. 1299–1313, 2010.

[27] "IEEE guide for improving the lightning performance of transmission lines," *IEEE Std 1243-1997*, pp. 1–44, 1997.

[28] Z. G. Datsios, P. N. Mikropoulos, and T. E. Tsovilis, "Closed-form expressions for the estimation of the minimum backflashover current of overhead transmission lines," *IEEE Trans. Power Del.*, vol. 36, no. 2, pp. 522–532, 2021.

[29] ——, "Effects of lightning channel equivalent impedance on lightning performance of overhead transmission lines," *IEEE Trans. Electromagn. Compat.*, vol. 61, no. 3, pp. 623–630, 2019.

[30] Z. G. Datsios, D. G. Patsalis, P. N. Mikropoulos, and T. E. Tsovilis, "Effects of lightning current waveform on the fast-front overvoltages and critical currents causing insulation flashover to a 150 kv overhead transmission line," in *Proc. 36th Int. Conf. Lightn. Prot. (ICLP)*, 2022.

[31] T. A. Papadopoulos, Z. G. Datsios, A. I. Chrysochos, P. N. Mikropoulos, and G. K. Papagiannis, "Wave propagation characteristics and electromagnetic transient analysis of underground cable systems considering frequency-dependent soil properties," *IEEE Trans. Electromagn. Compat.*, vol. 63, no. 1, pp. 259–267, 2021.